Title

Confocal Shear Wave Acoustic Radiation Force Optical Coherence Elastography for Imaging and Quantification of the In Vivo Posterior Eye

Journal

IEEE Journal of Selected Topics in Quantum Electronics, 25(1)

ISSN

1077-260X

Authors

He, Youmin

Qu, Yueqiao

Zhu, Jiang

et al.

Publication Date

2019

DOI

10.1109/jstqe.2018.2834435

Confocal Shear Wave Acoustic Radiation Force Optical Coherence Elastography for Imaging and Quantification of the *In Vivo* Posterior Eye

Youmin He, Yueqiao Qu, Jiang Zhu, Yi Zhang, Arya Saidi, Teng Ma, Qifa Zhou, and Zhongping Chen

***Abstract*—Retinal diseases, such as age-related macular degeneration (AMD), are the leading cause of blindness in the elderly population. Since no known cures are currently present, it is crucial to diagnose the condition in its early stages so that disease progression is monitored. Recent advances show that the mechanical elasticity of the posterior eye changes with the onset of AMD. In this paper, we present a quantitative method of mapping the mechanical elasticity of the posterior eye using confocal shear wave acoustic radiation force optical coherence elastography. This technique has been developed and validated with both an *ex-vivo* porcine tissue model and a customized *in vivo* rabbit model, which both showed the quantified elasticity variations between different layers. This study verifies the feasibility of using this technology for the quantification and diagnosis of retinal diseases from the *in vivo* posterior eye.**

***Index Terms*—Shear wave elastography, ARF, OCT, retina, *in vivo* study.**

I. Introduction

AGE-RELATED macular degeneration (AMD) is a progressive disease of the retina and is the leading cause of severe vision loss in the western population over 50 years of age [1]. AMD most often induces drusen formation in the dry form, and neovascularization in wet AMD. Drusen is present in more than half of the population over 70 years of age and often acts as an early sign of AMD [2]. Neovascularization occurs when excess blood vessels leak into the layers of the retina, signifying a later stage of disease. Although age is the primary factor that contributes to AMD, there are a number of environmental and genetic factors that are also associated and contribute to the onset and progression of AMD, including smoking, obesity, sunlight exposure, etc. [3].

Current methods of diagnosis include fundus photography, which provides surface structural information of the retina, and fluorescein angiography, which is used to visualize blood vessels and leakages if neovascularization is suspected [4]. For more accurate visualization of the entire depth of the retinal layers, optical coherence tomography (OCT) is used for non-invasive optical imaging [5]. OCT angiography is also used to produce the en face images of retinal blood vessels and diagnose abnormal regions. Once AMD is diagnosed, there is currently no known cure so disease management is necessary in various forms, including antiangiogenic drugs, radiation and laser treatments, and photodynamic therapy [6]. Since it is important to slow down the progression of the disease through treatment, early diagnosis is essential. Although it is possible to see anatomical changes that occur with drusen formation and neovascularization. It is very difficult to diagnose in the early stages, before structural changes are evident.

Recent studies show that the mechanical properties of the posterior eye also change with the onset of disease, such as in the case of angiogenesis or retinal degeneration [7]–[8]. In particular, the mechanical stress on the retina gets altered during the early stages when drusen deposits begin to form and also later when blood vessels infiltrate. Since it is often difficult to visualize drusen when the deposits are on the micron level, it would be helpful to use an alternate means of diagnosis [9]. In addition, since the layers of the posterior eye are made of a tight network of cells and tissues, the elasticity of different layers is expected to differ [8], [10].

Several methods for *in-vivo* measurements of mechanical properties of the eye have been reported [8], [10]–[11]. Elastography methods based on magnetic resonance imaging, ultrasound, and optical coherence tomography, have been widely used in determining the elasticity of tissues [12]–[19]. Optical coherence elastography (OCE) has the advantage in ocular imaging due to its high resolution ($<$10 um) and the transparency of ocular tissues [20]–[23]. However, few investigations of the mechanical properties of the posterior eye have been reported. *Ex-vivo* retinal elasticity has been studied previously,

Manuscript received December 12, 2017; revised February 23, 2018 and April 2, 2018; accepted May 1, 2018. Date of publication May 8, 2018; date of current version June 8, 2018. This work was supported in part by the National Institutes of Health under Grant R01HL-125084, Grant R01HL-127271, Grant R01EY-026091, Grant R01EY-021529, Grant P41EB-015890, Grant F31EY-027666, and Grant R01EY-028662, and in part by the Air Force Office of Scientific Research under Grant FA9550-14-1-0034. *(Y. H. and Y. Q contributed equally to this work and are treated as cofirst authors.) (Corresponding authors: Zhongping Chen and Qifa Zhou.)*

Y. He, Y. Qu, J. Zhu, and Z. Chen are with the Department of Biomedical Engineering and the Beckman Laser Institute, University of California, Irvine, CA 92697 USA (e-mail: youminh1@uci.edu; yueqiaoq@uci.edu; jzhumail@gmail.com; z2chen@uci.edu).

Y. Zhang, T. Ma and Q. Zhou are with the Department of Ophthalmology and Biomedical Engineering, Roski Eye Institute, University of Southern California, Los Angeles, CA 90089 USA (e-mail: zhangyi5757@hotmail.com; mt880501@gmail.com; qifazhou@usc.edu).

A. Saidi is with the Southern California College of Optometry, Marshall B. Ketchum University, Fullerton, CA 92831 USA (e-mail: aryasaidi@gmail.com).

Color versions of one or more of the figures in this paper are available online at http://ieeexplore.ieee.org.

Digital Object Identifier 10.1109/JSTQE.2018.2834435

where elasticity of only two different retinal layers were visualized and quantified based on shear wave OCE using a phased array transducer as excitation [24]. However, their ultrasound excitation and OCT detection are on the opposite side, and this configuration is not feasible for *in-vivo* animal studies where the posterior side is not accessible. Therefore, we propose this confocal shear wave acoustic radiation force optical coherence elastography (SW-ARF-OCE) system, where an ultrasound ring transducer and optical scan head are co-aligned to facilitate *in-vivo* study of the retinal elasticity. Although *in-vivo* corneal elastography studies have been performed, due to the difficulty in penetrating to the posterior globe through the anterior eye and vitreous combined with the need for high sensitivity and resolution, *in-vivo* measurements of the retinal stiffness have yet to be studied.

In this study, we report on the development of a shear wave ARF-OCE system that enables *in-vivo* imaging of the mechanical properties of the retina. To the best of our knowledge, we demonstrate the first *in-vivo* elasticity mapping of the retina. A rabbit model was measured, and the elasticities of the different retinal layers were identified in increasing stiffness from the ganglion side to the photoreceptor portions.

II. Materials and Methods

A. System Setup

A customized 50 kHz spectral domain optical coherence tomography (SD-OCT) system with a central wavelength of 890 nm and bandwidth of 144 nm is used for the detection of tissue structure and response to stimulation. The imaging depth range is 2.9 mm while the penetration depth in tissue is approximately 1.5 mm. The light emitted from the superluminescent diode is filtered through the optical isolator and split with an optical coupler. For the safety purpose of *in-vivo* retinal imaging, 20% of the light is transmitted to the sample, which is well within the ANSI safety limits, and 80% is redirected to a reference mirror. Glass imaging windows are placed in the stationary reference arm for dispersion compensation. In the sample arm, galvo mirrors are used for B-M mode scanning, and a scan lens is used with a focal length of 54 mm to penetrate through the ring transducer and into the posterior eye globe. The scattering signal from the sample arm is coupled together with the reflected reference arm signal and sent to the detector arm. The interference signal is separated by wavelength with a diffraction grating and focused onto a line scan CMOS camera. The signal is processed and transformed into depth-resolved intensity and phase information.

A 4.5 MHz ring ultrasound transducer was used for pulsed tissue excitation. The excitation duration was limited to 1–2 ms while the optical detection speed was 50 kHz. The optical setup and the *ex-vivo* sample setup are shown in Fig. 1(a), where a phosphate buffered saline (PBS) is used as the medium for ultrasound propagation as well as preservation of ocular tissue. For *in-vivo* experiments, the rabbit eye is proptosed within a rubber drape that can serve as a container to immerse the eye in PBS fluid as shown in Fig. 1(c). The ultrasound transducer was removed in Fig. 1(c) in order to visualize the ocular proptosis

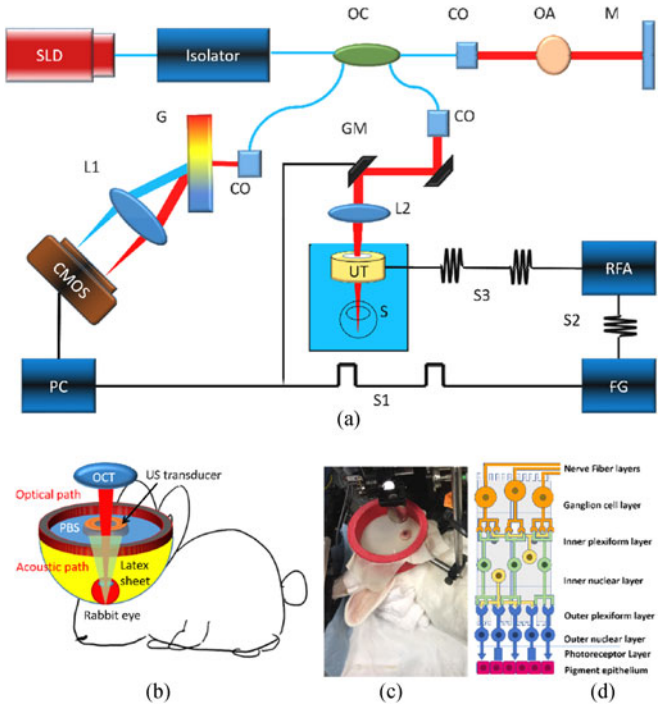

Fig. 1. System set up. (a) SW-ARF-OCE system schematic with *ex-vivo* sample. SLD: superluminescent diode, OC: optical coupler, CO: collimator, OA: optical attenuator, M: mirror, GM: galvanometer mirrors, L1/L2: lens, UT: ultrasound transducer, S: sample, RFA: radiofrequency amplifier, FG: function generator, G: grating, S1: baseband signal, S2: modulated signal, S3: amplified modulated signal. (b) Schematic of *in vivo* experimental setup. (c) Photograph of *in vivo* rabbit experimental setup. (d) Schematic of retina-layered anatomy.

of the rabbit. The drape system imitates the steridrapes that are used in clinical ultrasound. PBS is then added to the draped construct once again to serve as the medium for propagation as well as for lubrication of the rabbit eye. A detail description of this drape system can be illustrated in Fig. 1(b).

B. System Synchronization

For the shear wave excitation, a baseband signal (S1) is given by the PC to the function generator, which converts it into a sinusoidal modulated pulse signal with 1–2 msec duration. This pulse is amplified by approximately 42 dB and fed to the ultrasound transducer. A ultrasound generated pressure is applied onto the sample, initiating the propagation of the shear wave from the focal region to the peripheral areas. The detection scanning scheme is shown in Fig. 2(a), where the ultrasound excitation beam is given at location P0, and B-M mode detection occurs along the lateral direction from P1 to Pn. At each location, an excitation pulse of 1–2 ms is given and a series of 400 A-lines, which corresponds to 8.8 ms, is obtained in M mode before the galvanometer moves to the next location. The number of A-lines is chosen such that the entire duration and progression of the shear wave can be captured.

In order to achieve efficient and effective imaging, the entire excitation and detection process must be synchronized. The timing diagram is shown in Fig. 2(b). To obtain a B-scan showing the full lateral scanning area, an ultrasound modulation pulse is given for every 400 A-lines while the camera DAQ trigger is

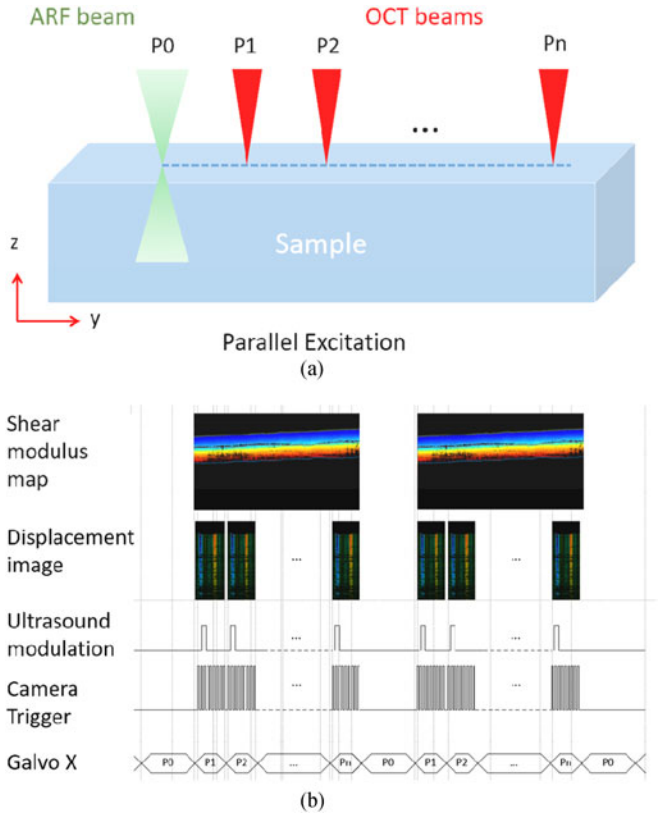

Fig. 2. (a) Scanning scheme of SW-ARF-OCE system. (b) Timing diagram.

given for each A-line to capture the intensity and phase information at each location for 8.8 ms total, in increments of 22 us. This synchronization generates 400 B-Scan images with lateral dimension of 600 um in a total of approximately 3.5 s. After detection is completed, the galvanometer moves to the next location in increments of 1.5 um, which is well within the lateral resolution of the optical system. The M-mode displacement image is obtained at every B-scan location, and the phase-resolved displacement is post-processed to obtain the shear modulus map. SW B-scan images are generated by reslicing the M-scan images, and therefore all the B-Scan images are generated at the same time after the imaging is completed.

C. Imaging Processing

Within the 400 A-lines in M-mode at each location, the entire shear wave propagation through that point can be captured. In Fig. 3(a)–(c), a sample raw data for the porcine retina is shown where it is apparent that different locations on the retina correspond to different propagation speeds. Note that only 330 out of 400 A-lines were shown in the figure below for visualization purpose. The transducer focal area is on the left side of the images, and propagation is to the right. For example, the bottom most layer of the retina propagates the fastest and corresponds to a stiffer tissue component. It is also important to note that the ultrasound wave intensity decreases at regions of stiffer tissue, and the intensity of the displacement is not considered in the velocity calculations.

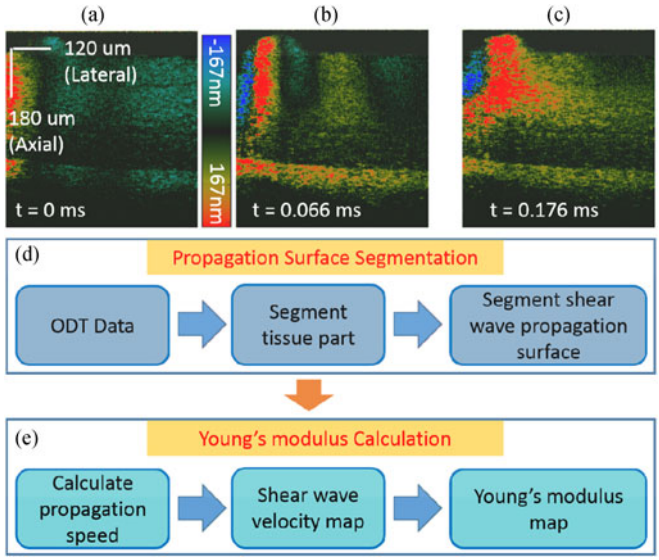

Fig. 3. (a–c) Cross-sectional raw data showing wave propagation of retinal layers at different time points for an *ex-vivo* pig retina. Shear wave induced axial displacement is shown by different colors corresponding to the color bar. (d–e) Flow diagram demonstrating postprocessing of raw data. DOCT: Doppler optical coherence tomography.

One of the challenges in analyzing retinal OCE data is segmentation. It is necessary to segment the boundaries across layers so that data from each individual layer can be isolated for layer specific elasticity analysis. Another challenge of shear wave elasticity analysis is to trace the location of the wave surface over time for the purpose of wave speed calculation. With layered Doppler OCT data and the segmentation algorithm, the wave surface as a function of time in each layer can be segmented to calculate the shear wave velocity at every location.

In the SW-ARF-OCE setup, the raw data is obtained, and postprocessing is performed to segment the layers and calculate the shear wave propagation speed. As shown in Fig. 3(d)–(e), the OCT intensity and Doppler phase data are first obtained, and the OCT image is segmented based on a customized dynamic programming segmentation algorithm to isolate different retinal layers [25]. Then the segmented layers are applied to the displacement map, where the shear wave propagation surfaces for each layer is segmented as well. Next, the propagation speed is calculated for each location based on the slope of the segmented wave propagation for each layer. The velocity is based on the change in location over the time period, and the shear wave velocity map can be obtained. The relationship between the velocity C_s and the shear modulus μ can be described with the equation $\mu = \rho {C_s}^2$ where ρ is the tissue density of approximately 1 kg/ m^3. The elastic modulus is approximately 3 times the shear modulus as demonstrated by previous literature [26] and can be calculated and mapped out as an elastogram.

D. Ex-Vivo Porcine Eye Preparation

The porcine eyeball was obtained within 24 hours of death. Since the eyeball was no longer fully transparent due to degradation, the anterior portion of the eye, including the cornea and the lens was removed along the iris. The vitreous was still

attached to the retina and was kept in place during imaging to avoid retinal detachment. A 0.8% agar phantom was moulded around the posterior globe and used to keep the eye in place during imaging as well as to help preserve the shape of the posterior globe and prevent detachment. The sample was kept in phosphate-buffered saline during imaging to preserve freshness and as a medium for ultrasound propagation.

E. In-Vivo Rabbit Experiment Preparation

All rabbit experiments were performed according to the University of California, Irvine (UCI) Institutional Animal Care and Use Committee (IACUC) protocol. The rabbit was used for an AMD study, where it was exposed to a high fat diet, blue light, and nicotine for 8 weeks. Since the disease was localized, most of the central retina was still relatively healthy. The healthy region was used for this study. The rabbit was given 35 mg/kg of ketamine and 5 mg/kg of xylazine subcutaneously for initial anesthesia. Two drops of proparacaine HCl and atropine solution were applied topically for further anesthesia and dilation of the eye for imaging, respectively. The unconscious rabbit was propped onto the imaging stage and the eye was proptosed. Additional anesthesia was given via subcutaneous injection of ketamine (17.5 mg/kg) if the heart rate or oxygen levels indicate distress. After imaging was completed, the rabbit was euthanized with an intravenous injection of euthasol. When death was confirmed, the rabbit eye was enucleated and fixed in 10% buffered formalin for histological analysis.

III. Results

A. Ex-Vivo Porcine Study

In order to test the confocal excitation and detection setup, imaging was first performed on an *ex-vivo* porcine retina using the same OCT system. The central retina region approximately 2 mm from the optic nerve on the temporal side was identified and imaged. The shear wave travels for over 700 um in the *ex-vivo* porcine retinal tissue and the system is capable of visualizing wave propagation in the whole depth of view. The results are shown in Fig. 4. The OCT intensity map is shown in Fig. 4(a) where segmentation was performed, and 5 different layers were isolated. Next, the corresponding shear wave velocity map and elastogram were calculated according to the above algorithm and shown in Fig. 4(b) and (c), respectively. Finally, an H&E histology slide of a porcine retina is shown in Fig. 4(d), where the 5 layers could be matched. Layer iv was omitted during the analysis due to low OCT scattering signal in the outer nuclear layer. Retinal detachment was observed and most likely due to detachment during the removal of the anterior portion and also due to the histology process.

The elasticity results of the porcine retina are summarized in Table I, where the mean and standard deviations for each layer are listed and plotted. The elasticity increased from approximately 6 kPa on the ganglion side to over 140 kPa on the photoreceptor side. Since the photoreceptor side is close to the sclera of the eye globe, it is expected to be stiffer. The close-knit structure of the retinal layers most definitely interferes with the mechanical elasticity for each and is demonstrated by the gradual gradient increase in the elasticity over the layers from the ganglion side to the photoreceptors.

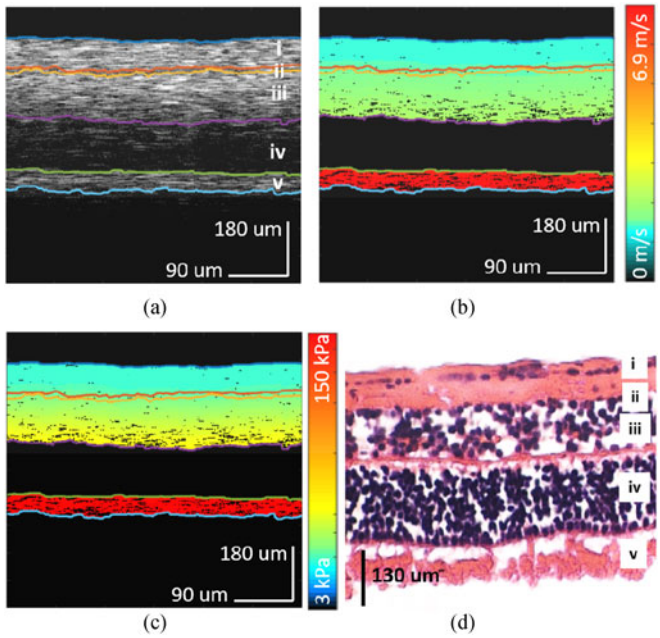

Fig. 4. *Ex-vivo* porcine retina results. (a) OCT of porcine central retina. (b) Velocity map of the shear wave propagation. (c) Elastogram of the corresponding region. (d) H&E staining of the porcine retinal layers. i: Optic nerve fibers (ONF) & ganglion cell layer (GCL); ii: inner plexiform layer (IPL); iii: inner nuclear layer (INL) & outer plexiform layer (OPL); iv: outer nuclear layer (ONL); v: photoreceptors (PR).

TABLE I
SUMMARY OF *Ex-Vivo* ELASTICITY MAPS OF EACH PORCINE RETINAL LAYER

Layer	Mean	Std
ONF&GCL	5.8	0.3
IPL	6.7	0.26
INL&OPL	10	1.97
ONL	N/A	N/A
PR	143	4.18

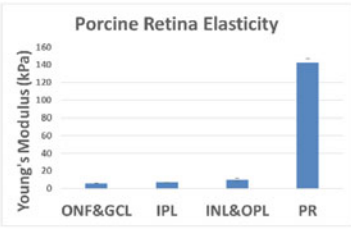

ONL has been omitted due to low OCT signal in the outer nuclear layer. SD: Standard deviation.

B. in-vivo Rabbit Study

Although the elasticity contrast between different retinal layers is apparent in the *ex-vivo* porcine model, the presence of intraocular pressure and blood vessel perfusion is lost. Therefore, it is not an accurate representation of the retinal structure in its natural environment. In order to address these issues, an *in-vivo* rabbit model was designed and imaged. For this shear wave elastography study, a healthy region of the central retina was chosen. The rabbit was put under anesthesia according to protocol and proptosed in the imaging setup as shown in Fig. 1(c).

Imaging was performed on the central retina approximately 1.5 mm from the optic disc on the temporal side. The same

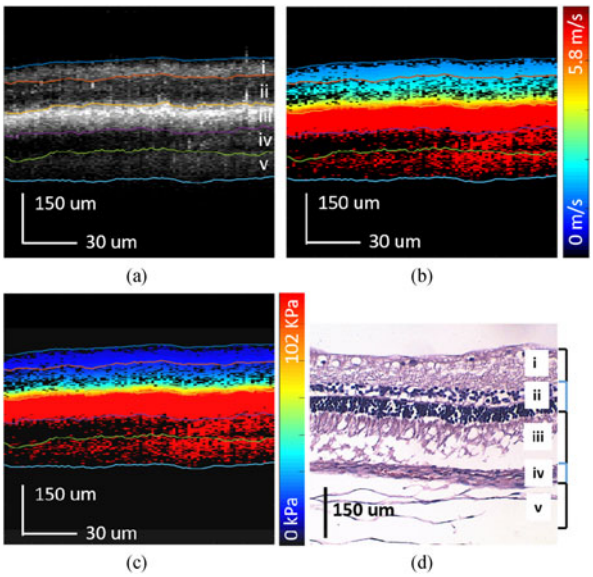

Fig. 5. *In vivo* rabbit elastography results. (a) OCT of rabbit central retina. (b) Shear wave velocity map. (c) Elastogram of corresponding region. (d) H&E histology showing some retinal detachment. i: Nerve fiber, ganglion cell, & inner plexiform; ii: inner nuclear, outer plexiform, & outer nuclear; iii: RPE; iv: choroid; v: sclera.

B-M mode scanning scheme was used to capture the shear wave propagation. The OCT intensity image is shown in Fig. 5(a), where segmentation was performed to isolate 5 different layers in the posterior globe. The shear velocity map is demonstrated in Fig. 5(b), and a speed of up to 5.8 m/s can be visualized. The velocity was converted to the Young's modulus in Fig. 5(c). The elasticity of the first three layers from the ganglion side to the photoreceptor side are: $12.6 \pm 1.5, 35.7 \pm 18.9, 101.1 \pm 5.1$ kPa. The bottom two layers of the eye could not be differentiated due to the fast propagation speed where the Young's modulus is over 100 kPa. The shear wave is attenuated within 200 um in the lateral direction and the current system setup is not fast enough to capture the wave propagation within such a distance for the bottom three layers. This issue can be resolved by increasing the imaging speed or extending the traveling distance of the shear wave with a higher ultrasound excitation power. According to the histology, the bottom two layers are close to the sclera and are expected to be stiffer than the retina and have a higher propagation velocity.

After the rabbit was euthanized, the posterior globe was fixed and processed for histological analysis. H&E staining is shown in Fig. 5(d), where the layers of the retina can be corresponded to the OCT figure similar to literature [27]. The retinal detachment is likely a fixation artifact while the swelling in the sclera or layer v is caused by the repeated proptosis procedure. Three layers of the live rabbit retina have been distinguished with different elasticity values. The feasibility of using the SW-ARF-OCE method to probe the mechanical properties of the retina has been confirmed.

IV. Discussion and Conclusion

We have presented a SW-ARF-OCE method of measuring and quantifying the *in-vivo* elasticity map of the retina for the first time, to the best of our knowledge. This technology offers high resolution imaging and highly sensitive velocity maps that are used to quantitatively assess retinal layers. Furthermore, the confocal setup allows for easy access to the posterior eye during the *in-vivo* study. In addition, the system is non-invasive since OCT and ultrasound are readily used in ophthalmic clinics today. Ultrasound gel and steridrape based waterbaths are commonly used in clinics to couple ultrasound into the eye and are adaptable in the translation of our technology. This technology will allow researchers and physicians to study the mechanisms behind changes in the mechanical elasticity of the retina during disease onset and progression, which is crucial in both basic pathological research as well as clinical diagnosis.

Although the quantification of retinal mechanical properties has been demonstrated *in-vivo*, a few challenges remain to be addressed before the technology can be translated. First, a higher imaging speed is necessary to visualize stiffer posterior layers, such as the sclera. A faster line scan camera can address this issue. A faster line scan camera will help speed up the scan time and allow for spatial imaging of a single ARF pulse. The temporal resolution of shear wave propagation will be increased so that faster shear wave speeds can be tracked within stiffer tissue such as the sclera. Second, the propagation distance of the shear wave is limited to a few hundred microns due to the fast attenuation of the signal. A larger field of view can be achieved with a high power excitation pulse, more precise confocal alignment of the ultrasound excitation on retinal tissue, or more ideally, the implementation of an array transducer for a larger region of excitation and detection. It is also important to study the changes in the mechanical properties using a diseased model and examine its correlation to clinical impairments.

The mechanical index (MI) of the current system exceeds the federal ophthalmic ultrasound limit (0.23) by approximately 10 fold. However, since we use phase-Doppler to measure the displacement in hundreds-nanometer range and the displacement sensitivity of this imaging system is less than 1 nm [28], it will be possible to scale down the excitation ARF by at least 1 order of magnitude and still obtain sufficient signal. In addition, it will be possible to measure the shear wave propagation across a spatial region using a single pulse with the incorporation of a faster camera. This will also decrease the patient exposure to ARF and help the translation of this technique to clinics. In addition, our current OCT image is not optimal due to the bulk motion and noise that occurs during *in-vivo* imaging. There is a significant amount of bulk motion from the rabbit breathing and reflex motions. Furthermore, since imaging took place in a PBS bath, some signal loss was observed. Imaging in fluids also changes the natural focal characteristics of the rabbit eye since the refractive index change from air to cornea is different than that from PBS to cornea, so it is more difficult to obtain a perfect focus on the retina. The *in-vivo* optical setup may be improved by considering the use of ophthalmic gel to substitute for the PBS bath, fine tuning the optical focus, and also bulk motion removal.

In conclusion, we have demonstrated a novel method to quantify the mechanical elasticity of the retinal layers *in-vivo* using SW-ARF-OCE based on layer segmentation and shear wave analysis. We have first tested the feasibility on an *ex-vivo* porcine

model, where 5 different retinal layers have been isolated and the mechanical elasticity was distinguished. In order to validate the feasibility of translating this technology, imaging was performed on an *in-vivo* New Zealand white rabbit retina model, where 3 layers of the retina could be analyzed and quantified for different mechanical properties. This study is a crucial stepping stone to the translation of the SW-ARF-OCE technology for clinical diagnosis and disease studies.

ACKNOWLEDGMENT

The authors would like to thank Dr. D. Minckler for his help in histological analysis. Dr. Z. Chen has a financial interest in OCT Medical Imaging Inc., which, however, did not support this work.

REFERENCES

[1] R. D. Jager, W. F. Mieler, and J. W. Miller, "Age-related macular degeneration," *New England J. Med.*, vol. 358, no. 24, pp. 2606–2617, 2008.
[2] N. M. Bressler, S. B. Bressler, and S. L. Fine, "Age-related macular degeneration," *Survey Ophthalmology*, vol. 32, no. 6, pp. 375–413, 1988.
[3] L. S. Lim, P. Mitchell, J. M. Seddon, F. G. Holz, and T. Y. Wong, "Age-related macular degeneration," *The Lancet*, vol. 379, no. 9827, pp. 1728–1738, 2012.
[4] U. Chakravarthy, J. Evans, and P. J. Rosenfeld, "Age related macular degeneration," *Bmj*, vol. 340, no. 7745, pp. 526–530, 2010.
[5] M. R. Hee *et al.*, "Optical coherence tomography of age-related macular degeneration and choroidal neovascularization," *Ophthalmology*, vol. 103, no. 8, pp. 1260–1270, 1996.
[6] L. Cour, M. Jens, F. Kiilgaard, and M. H. Nissen, "Age-related macular degeneration," *Drugs Aging*, vol. 19, no. 2, pp. 101–133, 2002.
[7] L. Krishnan, J. B. Hoying, H. Nguyen, H. Song, and J. A. Weiss, "Interaction of angiogenic microvessels with the extracellular matrix," *Amer. J. Physiology Heart Circulatory Physiology*, vol. 293, pp. H3650–H3658, 2007.
[8] K. Chen, A. P. Rowley, and J. D. Weiland, "Elastic properties of porcine ocular posterior soft tissues," *J. Biomed. Mater. Res. Part A*, vol. 93, no. 2, pp. 634–645, 2010.
[9] S. H. Sarks, J. J. Arnold, M. C. Killingsworth, and J. P. Sarks, "Early drusen formation in the normal and aging eye and their relation to age related maculopathy: A clinicopathological study," *Brit. J. Ophthalmology*, vol. 83, no. 3, pp. 358–368, 1999.
[10] T. R. Friberg and J. W. Lace, "A comparison of the elastic properties of human choroid and sclera," *Exp. Eye Res.*, vol. 47, no. 3, pp. 429–436, 1988.
[11] I. L. Jones, M. Warner, and J. D. Stevens, "Mathematical modelling of the elastic properties of retina: a determination of Young's modulus." *Eye*, vol. 6, no. 6, pp. 556–559, 1992.
[12] D. V. Litwiller *et al.*, "MR elastography of the ex vivo bovine globe," *J. Magn. Resonance Imag.*, vol. 32, no. 1, pp. 44–51, 2010.
[13] J.-L. Gennisson, T. Deffieux, M. Fink, and M. Tanter, "Ultrasound elastography: Principles and techniques," *Diagnostic Interventional Imag.*, vol. 94, no. 5, pp. 487–495, 2013.
[14] E. T. Detorakis, E. E. Drakonaki, M. K. Tsilimbaris, I. G. Pallikaris, and S. Giarmenitis, "Real-time ultrasound elastographic imaging of ocular and periocular tissues: A feasibility study," *Ophthalmic Surgery, Lasers Imag. Retina*, vol. 41, no. 1, pp. 135–141, 2010.
[15] S. Wang and K. V. Larin. "Shear wave imaging optical coherence tomography (SWI-OCT) for ocular tissue biomechanics," *Opt. Lett.*, vol. 39, no. 1, pp. 41–44, 2014.
[16] Y. Qu *et al.*, "Miniature probe for mapping mechanical properties of vascular lesions using acoustic radiation force optical coherence elastography," *Sci. Reports*, vol. 7, 2017, Art no. 4731.
[17] J. Zhu *et al.*, "Longitudinal shear wave imaging for elasticity mapping using optical coherence elastography," *Appl. Phys. Lett.*, vol. 110, no. 20, 2017, Art no. 201101.
[18] J. Zhu *et al.*, "3D mapping of elastic modulus using shear wave optical micro-elastography," *Sci. Reports*, vol. 6, 2016, Art no. 35499.
[19] J. Zhu *et al.*, "Imaging and characterizing shear wave and shear modulus under orthogonal acoustic radiation force excitation using OCT Doppler variance method," *Opt. Lett.*, vol. 40, no. 9, pp. 2099–2102, 2015.
[20] M. R. Ford, W. J. Dupps, A. M. Rollins, A. S. Roy, and Z. Hu, "Method for optical coherence elastography of the cornea," *J. Biomed. Opt.*, vol. 16, no. 1, pp. 016005–016005, 2011.
[21] Z. Han *et al.*, "Quantitative assessment of corneal viscoelasticity using optical coherence elastography and a modified Rayleigh–Lamb equation," *J. Biomed. Opt.*, vol. 20, no. 2, pp. 020501–020501, 2015.
[22] S. Wang and K. V. Larin, "Noncontact depth-resolved micro-scale optical coherence elastography of the cornea," *Biomed. Opt. Express*, vol. 5, no. 11, pp. 3807–3821, 2014.
[23] Y. Qu *et al.*, "Acoustic radiation force optical coherence elastography of corneal tissue," *IEEE J. Sel. Topics Quantum Electron.*, vol. 22, no. 3, pp. 288–294, May/Jun. 2016, Art. no. 6803507.
[24] S. Song, N. M. Le, Z. Huang, T. Shen, and R. K. Wang, "Quantitative shear-wave optical coherence elastography with a programmable phased array ultrasound as the wave source," *Opt. Lett.*, vol. 40, no. 21, pp. 5007–5010, 2015.
[25] S. Huang, Z. Piao, J. Zhu, F. Lu, and Z. Chen, *In vivo* microvascular network imaging of the human retina combined with an automatic three-dimensional segmentation method. *J. Biomed. Opt.*, vol. 20, no. 7, pp. 076003–076003, 2015.
[26] M. Razani *et al.*, "Feasibility of optical coherence elastography measurements of shear wave propagation in homogeneous tissue equivalent phantoms," *Biomed. Opt. Exp.*, vol. 3, no. 5, pp. 972–980, 2012.
[27] E. Cohen *et al.*, "Optical coherence tomography imaging of retinal damage in real time under a stimulus electrode," *J. Neural Eng.*, vol. 8, no. 5, 2011, Art no. 056017.
[28] J. Zhang, B. Rao, L. Yu, and Z. Chen, "High-dynamic-range quantitative phase imaging with spectral domain phase microscopy," *Opt. Lett.*, vol. 34, no. 21, pp. 3442–3444, 2009.

Youmin He received the B.S. and M.S. degrees from the School of Electronics and Information Engineering, Beijing Jiaotong University, Beijing, China, in 2011 and 2014, respectively, and the M.S. degree in biomedical engineering from the University of California, Irvine, CA, USA, in 2017. He is currently working toward the Ph.D. degree under the guidance of Dr. Z. Chen. His research interests include fast image segmentation, parallel computing for real time OCT imaging, high-resolution OCT system for airway imaging, and ARF-OCE technology development and application on ophthalmology and cardiology.

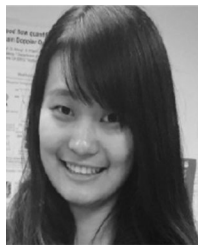

Yueqiao Qu received the B.S. degree in biomedical engineering from the Johns Hopkins University, Baltimore, MD, USA, and the M.S. degree in biomedical engineering from the University of California, Irvine, CA, USA, in 2011 and 2015, respectively. She is currently working toward the Ph.D. degree under the guidance of Dr. Z. Chen. Her research interests include ARF-OCE technology development and applications in ophthalmology and cardiology, integrated intravascular ultrasound (IVUS) and OCT imaging, and miniature optical fiber catheter development for photoacoustic imaging, IVUS-OCT, and ARF-OCE. She was the recipient of the National Institutes of Health T32 fellowship and the F31 grant.

Jiang Zhu received the Ph.D. degree in biology from Tsinghua University, Beijing, China, in 2009. He currently a Postdoctoral Researcher with Beckman Laser Institute, Irvine, CA, USA. His interests include optical coherence elastography and Doppler OCT.

Yi Zhang received the Ph.D. degree from the Department of Mechanical and Electrical Engineering, Xiamen University, Xiamen, China, in 2008. He is currently a Postdoctoral Research Associate with the Roski Eye Institute and the Department of Ophthalmology, University of Southern California (USC), Los Angeles, CA, USA. Before joining USC in 2012, he worked with the Division of Biomedical Engineering, University of Glasgow, Scotland, U.K. His research interests include the development of ophthalmic medical devices, MEMS technology, ultrasound transducers, and arrays for biomedical applications. He has published more than 30 journal papers in this area. He is a member of IEEE Ultrasonics, Ferroelectrics, and Frequency Control Society.

Arya Saidi received the B.S. degree in biomedical engineering from the University of California, Irvine, CA, USA, in 2010. He is currently a Doctor of Optometry Candidate with the Southern California College of Optometry, Fullerton, CA, USA, and continues his research in ophthalmic imaging at the Beckman Laser Institute and Medical Clinic, Irvine, CA, USA under the guidance of Dr. Z. Chen. He was the recipient of Chancellor's Award of Excellence in Undergraduate Research at UC Irvine. His research interests include ARF-OCE applications in optometry, the development of animal models for ophthalmic imaging, and OCT imaging.

Teng Ma received the B.S.E degree in biomedical engineering from the University of Michigan, Ann Arbor, MI, USA, in 2011, and the M.S. and the Ph.D. degrees in biomedical engineering from the University of Southern California, Los Angeles, CA, USA, in 2013 and 2015, respectively. He joined NIH Resource Center for Medical Ultrasonic Transducer Technology as a Research Assistant and a Ph.D. Candidate under the supervision of Dr. K. K. Shung and Dr. Q. Zhou. His research interests include medical ultrasound technology and multimodality intravascular imaging by combining ultrasonic and optical techniques, such as intravascular ultrasound (IVUS), intravascular optical coherence tomography (IV-OCT), intravascular photoacoustic imaging (IVPA), and acoustic radiation force optical coherence elastography (ARF-OCE). He is also actively working in translational research and on medical device commercialization with entrepreneurial spirit to translate innovative technology from research to clinical benefits. In 2013, two of his papers were selected as "Best Student Paper Finalist" and featured in the 2013 Joint UFFC, EFTF, and PFM symposium.

Qifa Zhou received the Ph.D. degree from the Department of Electronic Materials and Engineering, Xi'an Jiaotong University, Xian, China, in 1993. He is currently a Research Professor with the NIH Resource on Medical Ultrasonic Transducer Technology and the Department of Biomedical Engineering and Industry & System Engineering, University of Southern California (USC), Los Angeles, CA, USA. Before joining USC in 2002, he worked with the Department of Physics, Zhongshan University, Guangzhou, China, the Department of Applied Physics, Hong Kong Polytechnic University, and the Materials Research Laboratory, Pennsylvania State University. His research interests include the development of ferroelectric thin films, MEMS technology, nanocomposites, and modeling and fabrication of high-frequency ultrasound transducers and arrays for medical imaging applications, such as photoacoustic imaging and intravascular imaging. He has published more than 130 journal papers in this area. He is a fellow of International Society for Optics and Photonics (SPIE) and American Institute for Medical and Biological Engineering (AIMBE). He is also a senior member of the IEEE Ultrasonics, Ferroelectrics, and Frequency Control Society and a member of the UFFC Society's Ferroelectric Committee. He is a member of the Technical Program Committee of the IEEE International Ultrasonics Symposium. He is an Associate Editor of the IEEE TRANSACTIONS ON ULTRASONICS, FERROELECTRICS, AND FREQUENCY CONTROL.

Zhongping Chen received the B.S. degree in applied physics from Shanghai Jiao Tong University, Shanghai, China, the M.S. degree in electrical engineering from Cornell University, New York, NY, USA, and the Ph.D. degree in applied physics from Cornell University, in 1982, 1987, and 1993, respectively. He is currently a Professor of biomedical engineering and the Director of F-OCT Laboratory, University of California, Irvine, CA, USA. He is the cofounder and the Board Chairman of OCT Medical Imaging, Inc. His research group has pioneered the development of functional optical coherence tomography, which simultaneously provides high-resolution 3-D images of tissue structure, blood flow, and birefringence. He has published more than 250 peer-reviewed papers and review articles and holds a number of patents in the fields of biomaterials, biosensors, and biomedical imaging. His research interests include biomedical photonics, microfabrication, biomaterials, and biosensors. He is a fellow of the American Institute of Medical and Biological Engineering, a fellow of SPIE, and a fellow of the Optical Society of America.